PROFILE RECONSTRUCTION TECHNIQUES FOR THE JET NEUTRON AND GAMMA-RAY CAMERAS

Teddy Craciunescu, Ion Tiseanu, Vasile-Liviu Zoita

EURATOM-MEdC Association, National Institute for Lasers Plasma and Radiation Physics, Bucharest, Romania

1. Introduction

The JET neutron profile monitor is a unique instrument among neutron diagnostics available at large fusion research facilities. The profile monitor comprises two fan shaped multi-collimator cameras, with 10 channels in the horizontal camera and 9 channels in the vertical camera. A schematic drawing of the JET neutron emission profile monitor, showing the 19 lines of sight is presented in Fig. 1. Each line of sight is equipped with a set of three different detectors: i) a NE213 liquid organic scintillator with pulse shape discrimination (PSD) electronics for simultaneous measurements of the 2.5 MeV D-D neutrons, 14 MeV D-T neutrons and γ-rays, ii) a BC418 plastic scintillator, insensitive to γ-rays with $E\gamma$ < 10 MeV for the measurements of 14 MeV D-T neutrons and iii) a CsI(Tl) scintillation detector for measuring the hard X-rays and gamma emission in the range between 0.2 and 6 MeV. The collimation can be adjusted by use of two pairs of rotatable steel cylinders. The instrument has a time resolution currently of 10 ms.

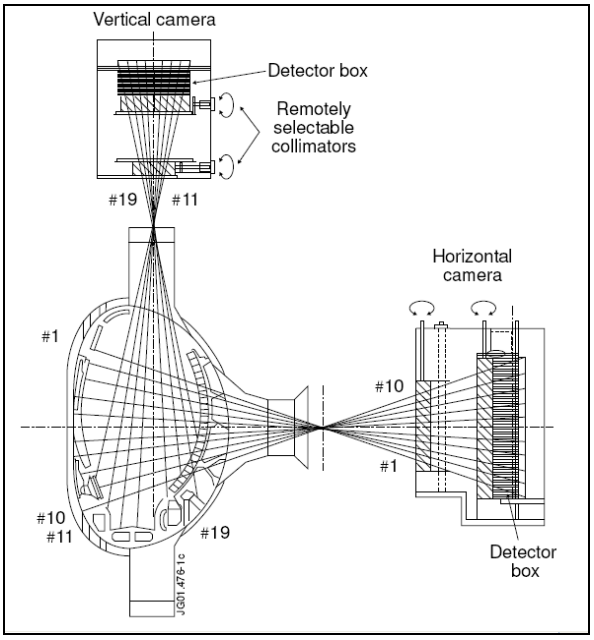

Figure 1. Schematic view of the JET neutron emission profile monitor showing the lines of sight.

The plasma coverage determined by the 19 line of sight can be used for neutron or γ-ray tomography. It ensures a 2D arrangement for measurements and distribution determination. The 2D slice is located in the plane defined by the major torus radius (R) and the major torus axis (Z). The thickness of the plasma slice along the toroidal direction, determined by the collimation system, is approximately 75 mm.

In 2-D tomography systems, measurements are taken along lines of sight, and can essentially be represented by line integrals; i.e. the measurement p is given by straight line integrals of the emissivity $f(x, y)$, where x and y are Cartesian coordinates of the plane. The emissivity function can be

appropriately discretized on a 2-D grid. For this purpose, the reconstruction area is divided into pixels that are sufficiently small for emissivity variations within a pixel to be negligible. The weight matrix W describes the geometrical layout of the detectors and its element w_{ik} indicates the contribution of the i*th* pixel to the k*th* detector. The basic set of tomographic equations is:

$$p_k = \sum_{i=1}^{N_p} w_{ik} \cdot f_i, \quad k = 1,2,\ldots, N_d \tag{1}$$

where N_p and N_d are the numbers of pixels and detectors, respectively. This set of linear equations represents the linear inverse problem. Obviously, even with exact data constraints, this inversion cannot be uniquely performed when there are fewer data than pixels, as is generally the case in plasma tomography.

The existence of only two views (projections in tomographic terms) and the coarse sampling in each projection leads to a highly limited data set tomographic problem. For example, in the case of a reconstruction grid with 20 x 35 pixels (pixel size of 90 x 90 mm) an image with 700 pixel values must be retrieved from 19 experimental data. In consequence special algorithms which are suitable and specific to the machine and its constrains, allowing effective tomography from the available limited data must be developed.

2. Methods

2.1 The ML reconstruction method

The ML method can be derived based on the principles of the Bayesian tomography. Let P represent a set of measured projection data, and let F represent a model of the object under consideration. The goal is to assign values to F that accurately reflect the objects being inspected from the noisy and potentially incomplete data, P. In ML estimation, the estimated model F_{ML} is taken to be the value of F which maximizes the likelihood, $L(P \mid F)$, of observing P, assuming that F is correct. Equivalently, and more commonly, the log-likelihood can be maximized. More precisely, in ML tomography, it is assumed that the emission is a Poisson process and p_k is a sample from a Poisson distribution whose expected value is:

$$\sum_k w_{ik} f_i \tag{2}$$

Then the probability of obtaining the measurement $P \equiv \{p_k \mid k = 1,\ldots N_d\}$ if the image is $F \equiv \{f_i \mid i = 1,\ldots N_p\}$ (the so-called likelihood function) is:

$$L(P/F) = \prod_k \left[\frac{1}{p_k!} \left(\sum_i w_{ik} f_i \right)^{p_k} \times \exp\left(- \sum_i w_{ik} f_i \right) \right] \tag{3}$$

The ML method solves the problem of evaluating *F*, if *P* is known, by selecting the particular *F* which maximizes *L(P/F)*. This is a difficult nonlinear optimization problem and until the application of the iterative expectation maximization (EM) algorithm by Shepp and Vardi [1] there was no method with known convergence properties for generating the ML solution. The iterative solution is given by the following formula:

$$f_i^{(iter+1)} = f_i^{(iter)} \frac{\sum_k w_{ik} \dfrac{p_k}{\sum_l w_{jl} f_j^{(iter)}}}{\sum_k w_{ik}} \tag{4}$$

where $f_i^{(iter)}$ is the reconstructed image for the iteration *iter*, *i* and *j* are image element indices, *k and l* are projection element indices.

A well known characteristic of the ML algorithm is that the unconstrained maximum-likelihood estimator has a fundamental noise artifact that worsens as the iterative algorithm climbs the likelihood hill. Even though the likelihood function is monotonically increasing with the iteration number, the best reconstruction is obtained before irregular high amplitude patterns or global distortions arise. In consequence, a criterion for optimal stopping of the algorithm must be introduced. We found that the correlation coefficient between reconstructions obtained at successive iterations reaches its maximum value for the best reconstruction.

2.2 The ML reconstruction method

As the tomographic problem is highly undetermined, the reconstruction algorithm can lead to a solution which satisfy Eq. 1 but has no physical relevance and may bring about wrong interpretations. A priori information about the expected emission profile, can be introduced in order to compensate for the lack of experimental information. Smoothness can be imposed on the solution of the tomographic problem as regularization. In order to prevent oversmoothing which may lead to the blurring of certain features in the reconstruction, it is necessary to find the smoothest function for which the misfit is equal to the estimated noise.

The smoothing operator is implemented as one-dimensional median filtering, using a sliding window which moves on the magnetic contour lines:

$$f_i = \sum_{\substack{j=-w_{med} \\ w_{med} \in L_k}}^{j=+w_{med}} m_{ji} h_j \tag{5}$$

where m_{ji} is the matrix which defines the window-based median filter, w_{med} is half of the width of filtering window and L_k designates a close magnetic contour line L_k. The iterative ML algorithm works directly on the reconstructed image which is successively updated. This allows image manipulation at each iteration for introducing *a priori* knowledge. Therefore smoothing is applied, as described, at each iteration. In order to obtain additional smoothing, we transformed the experimental projection by resampling, using spline interpolation. Projection resampling implies the introducing of virtual lines of sight which ensures an improved coverage of the reconstruction domain. By numerical simulations, we found that the effect of these smoothing techniques are strong enough to make useless the implementation of beam-width.

3. Results

The method was tested on numerically simulated phantoms with shapes characteristic for this kind of tomography and good quality reconstructions were obtained (Fig. 2).

Besides the qualitative evaluation (size, shape and resolution) of the reconstruction, some figures of merit were introduced in order to evaluate the performance of the ML method. The horizontal and vertical line profiles describe the variation of the image intensity along the horizontal and vertical axes of a coordinate system with the origin in the centre of the image. The main features of the image, for all phantoms, intersect these two axes. In consequence, the line profiles offer information mainly concerning the spatial resolution.

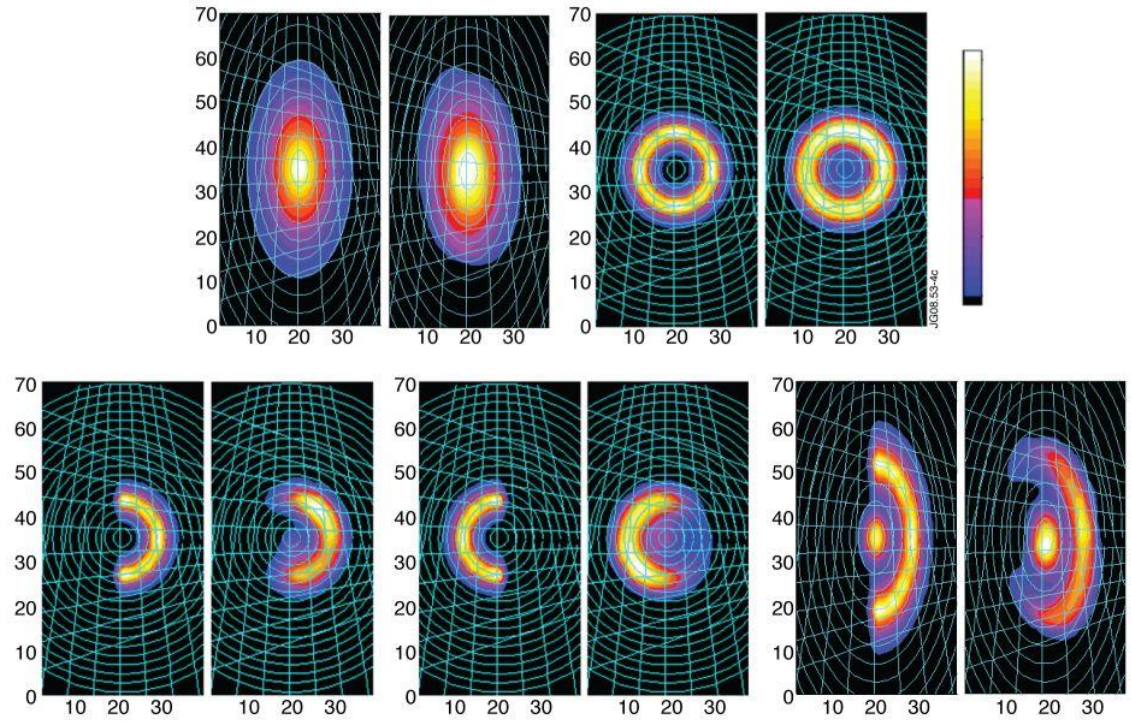

Figure 2 - The test phantoms and their ML reconstruction: peak (top-left), hollow (top-right), "banana" (bottom-left), symmetrically reversed "banana" (bottom-middle) and banana" plus peak (bottom-right). In each case the phantom is presented in the left side of the illustration and the reconstruction in the right one.

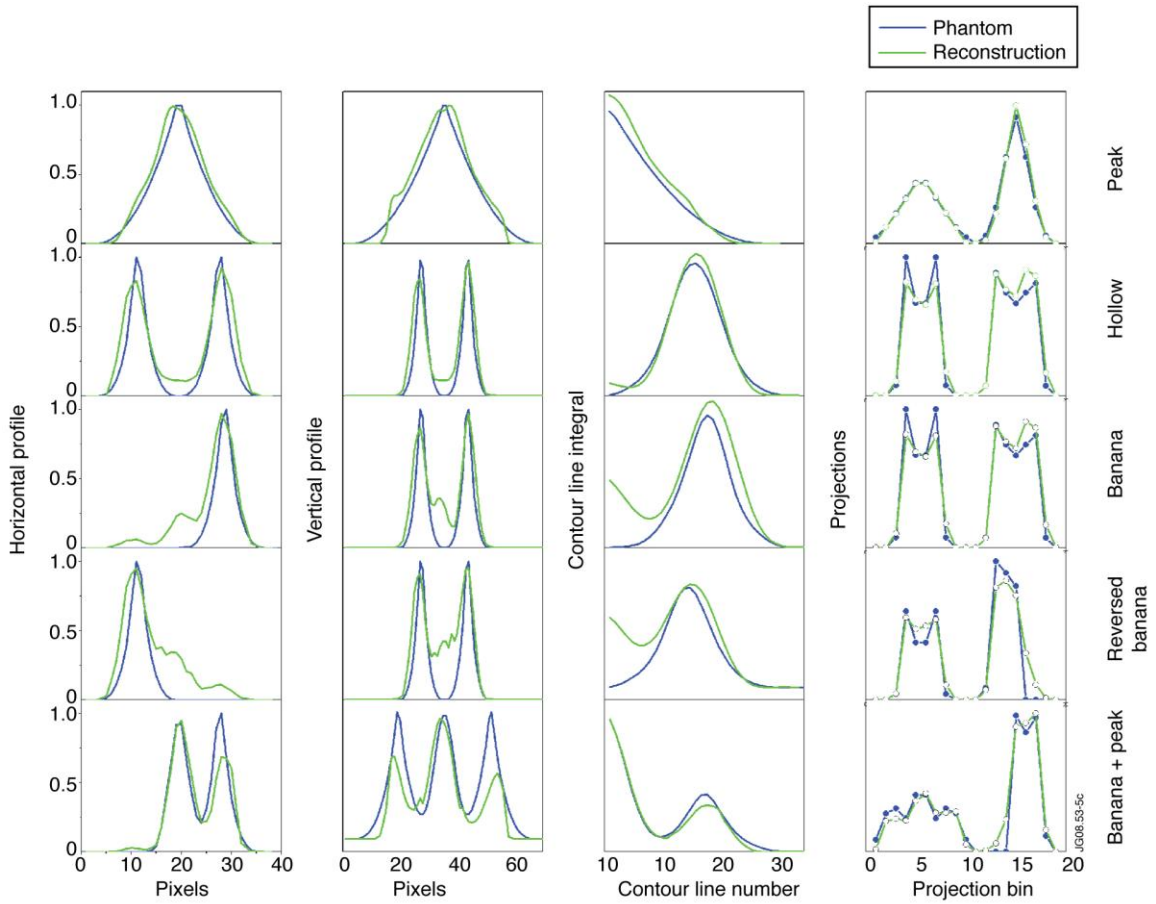

Figure 3 - Figures of merit; each row corresponds to a phantom – from top to bottom: peak, hollow, "banana", simmetrically reversed "banana", "banana" plus peak; each column corresponds to a specific figure of merit – from left to right: horizonthal line profile, vertical line profile, integrals along magnetic contour lines, projections calculated using the phantom and the reconstruction, respectively

Line integrals were calculated along the 35 magnetic contour lines, starting from the centre of the reconstruction and covering the whole image. The plot of these integrals, offers information about the quality of the shape and size reconstruction. A global evaluation of the reconstruction is given by the comparison of the initial projections and the projections calculated using the reconstruction obtained by ML method. All these figures of merit are presented in Fig. 3.

The method was applied for the analysis of experimental data recorded at JET and significant results are reported (Fig. 4). A *peak* type reconstruction is presented in Fig. 4 - left. This is the reconstructions of the DT-neutron emissivity profile in the experiment with the T-puff in the deuterium plasma at 62.5 s during the D neutral beam injection. In such experiments, tritium is injected in 'trace' amount (typically $n_T / n_T + n_D \lesssim 3\%$) and the temporal evolution of the tritium spatial distribution can be detected by observation of the 14 MeV neutron emission, allowing non-perturbative transients experiments. The neutron profile is a typical one for plasma with tritium which has penetrated to the plasma core in full. A "*banana*" type distribution (Fig. 4 – middle) corresponds to an experiment where the DT-neutron emission was measured in the ohmic deuterium discharge during the off-axis injection of the T neutral beam. The reconstruction of a combined *peak plus "banana"* distribution – most difficult case from the tomographic point of view - is illustrated in Fig. 4 - right. This profile was recorded just after the T-puff in the same discharge, and tritons partly penetrated to the plasma core from the periphery.

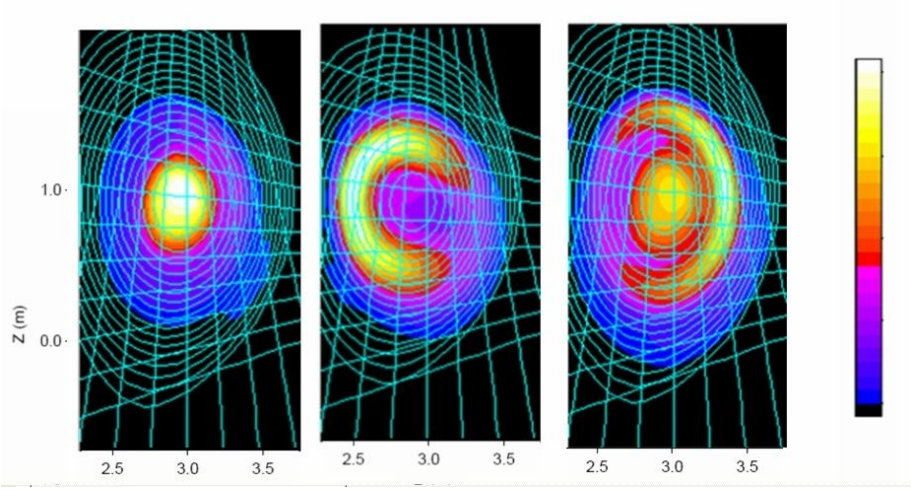

Figure 4 - DT-neutron emissivity profile reconstruction in an experiment with the T-puff in the deuterium plasma using ML method: peak profile distribution, typical for plasma with tritium which has penetrated to the plasma core in full - shot: 61132 at 62.92 s (left); "banana"profile distribution corresponding to an experiment where the DT-neutron emission was measured in the ohmic deuterium discharge during the off-axis injection of the T neutral beam – shot 61237 at 46.22 – 46.27s (middle); peak plus "banana" profile distribution recorded just after the T-puff, when tritons partly penetrated to the plasma core from the periphery – shot 61132 at 62.67 s (right).

Besides spatial information, tomography is able to provide also information about the temporal evolution of the neutron emissivity. The capability of the ML method to reveal this kind of information is illustrated in Fig. 5, where six reconstructions are taken in the temporal interval 60.87-61.32 s. They show the temporal evolution of the D-T 14 MeV neutron emissivity in a trace tritium experiment. The tomographic reconstruction demonstrates a relaxation of the high density plasma, which is heated by D neutral beams after the T-puff at 60.5 s. An evolution of the tritium penetration from the edge toward the core can be clearly seen.

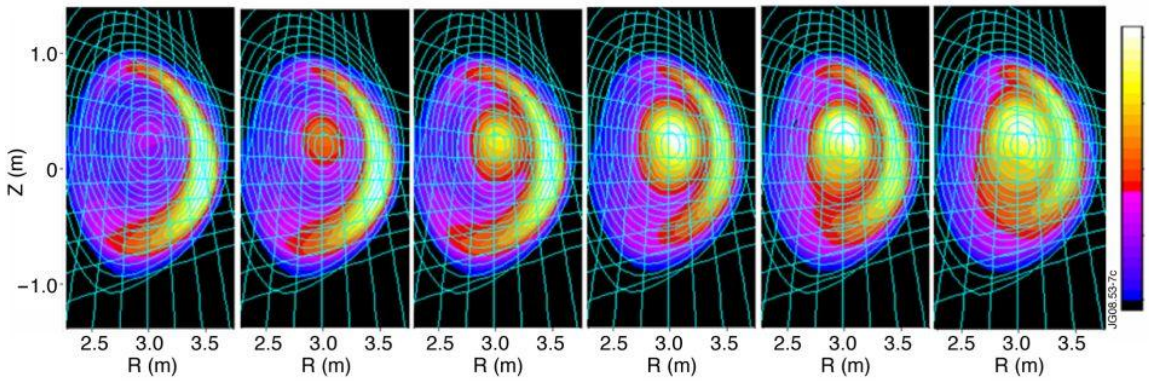

Figure 5 - Temporal evolution of the D-T 14 MeV neutron emissivity in a trace tritium experiment showing the relaxation of the high density plasma, which is heated by D neutral beams after the T-puff – ML reconstructions for shot 61141 (from 60.87 s to 61.32 s).

ML was used during JET campaingns C20-21 in experiments (1) M-3.3.3 - *Identify and document main fast ion loss mechanisms* and (2) M-3.3.1 - *Compare fast particle losses for various scenarios*. Reconstruction of γ-ray profiles: $E_{3He} > 0.9$ MeV, $^{9}Be(^{3}He,p\gamma)^{11}B$, $^{9}Be(^{3}He,n\gamma)^{11}C$, $^{12}C(^{3}He,p\gamma)^{14}N$ were performed for shots 73205-73214. Significant results are presented in Fig. 6. Experiment (2) represented a good opportunity to test the ability of the ML method to provide inter-shot tomographic analysis. The method succeeded to provide reconstructions for each shot (73761 – 73770), in between shots. This recommends the ML method as an appropriate method for inter-shot analysis.

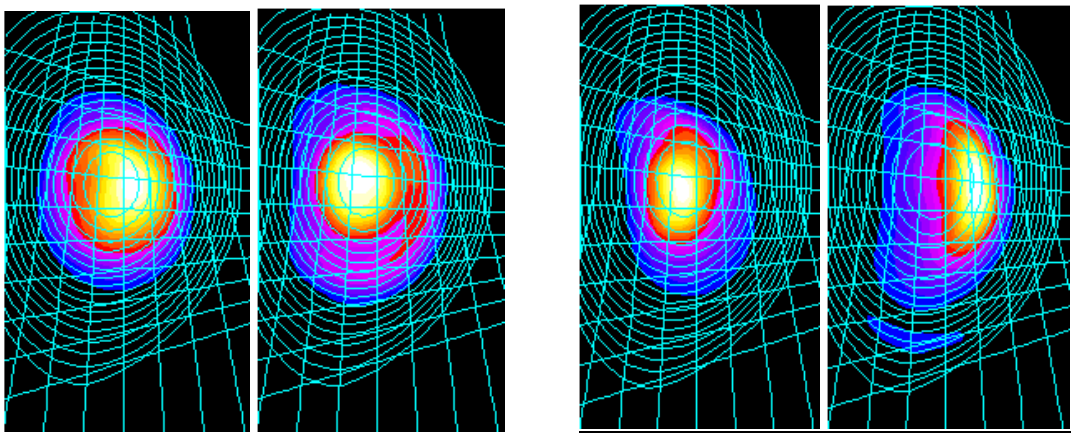

Figure 6 - Reconstruction obtained during experiment (1): shots 73205, 73213 (left) and reconstruction obtained during experiment (2): shots 73765, 73766 (right)

4. Conclusion

In conclusion we appreciate that the ML reconstruction method provides good reconstructions in terms of shapes and resolution. An efficient smoothing technique, is introduced in order to compensate for the lack of experimental information. The strategy used for smoothing implementation allows fast reconstructions. The possibility of further optimization qualifies ML as a candidate for inter-shot analysis.
The results obtained were published [2][3].The work on profile reconstruction techniques will be continued in 2009 with the assessment of the quality of the tomographic methods developed in frame of this project and software package development Also support in JET experimental campaigns will be provided.

References

[1] L.A. Shepp, Y. Vardi, “Maximum Likelihood Reconstruction for Emission Tomography”, IEEE Transactions on Medical Imaging, Vol. 1 (1982) 113 121.

[2] T. Craciunescu, G. Bonheure, V. Kiptily, A. Murari, S. Soare, I. Tiseanu, V. Zoita, *The Maximum Likelihood Reconstruction Method for JET Neutron Tomography*, Nuclear Inst. and Methods in Physics Research, A, 595, p. 623–630, 2008 (http://dx.doi.org/10.1016/j.nima.2008.07.145).

[3] V. G. Kiptily, S. D. Pinches, S. E. Sharapov, D. Borba, F. E. Cecil, D. Darrow, V. Goloborod’ko, T. Craciunescu, T. Johnson, F. Nabais, C. P. Perez von Thun, M. Reich, A. Salmi, V. Yavorskij, M. Cecconello, G. Gorini, P. Lomas, A. Murari, V. Parail, S. Popov. Recent Progress in Fast-Ion Physics on JET. In *Proc, of 22nd IAEA Fusion Energy Conference, 13-18 October 2008, Geneva, Switzerland*, pp. P8.8-1-8. 2008. (http://www-pub.iaea.org/MTCD/Meetings/FEC2008/ex_p8-8.pdf)